

Article

Effect of Alloying and Reinforcing Nanocomposites on the Mechanical, Tribological, and Wettability Properties of Pulse-Electrodeposited Ni Coatings

Aashish John, Adil Saeed  and Zulfiqar Ahmad Khan * 

NanoCorr, Energy & Modelling (NCEM) Research Group, Bournemouth University, Talbot Campus, Poole BH12 5BB, UK; ajohn@bournemouth.ac.uk (A.J.); asaheed4@bournemouth.ac.uk (A.S.)

* Correspondence: zkhan@bournemouth.ac.uk

Abstract: Research into the introduction of alloying and reinforcing nanocomposites into nickel (Ni) coatings has been motivated by the need for tribologically superior coatings that will improve energy efficiency. Using pulse electrodeposition, this work investigates the effects of adding cobalt (Co) as the alloying nanoparticle and silicon carbide (SiC), zirconium oxide (ZrO₂), and aluminium oxide (Al₂O₃) as reinforcing nanocomposites to Ni coatings. The surface properties, mechanical strength, nanotribological behaviour, and wettability of these coatings were analysed. Surface characteristics were evaluated by the use of a Scanning Electron Microscope, revealing a grain dimension reduction of approximately ~7–43% compared to pristine Ni coatings. When alloying and reinforcing nanocomposites were added to Ni coatings, nanoindentation research showed that there was an increase in nanohardness of ~12% to ~69%. This resulted in an improvement in the tribological performance from approximately 2% to 65%. The hydrophilic nature of Ni coatings was observed with wettability analysis. This study demonstrates that nanocomposite reinforcement can be used to customise Ni coatings for applications that require exceptional tribological performance. The results point to the use of Ni-Co coatings for electronics and aerospace sectors, with more improvements possible with the addition of reinforcing nanoparticles.



check for updates

Academic Editor: Nam-Trung Nguyen

Received: 12 November 2024

Revised: 27 January 2025

Accepted: 29 January 2025

Published: 31 January 2025

Citation: John, A.; Saeed, A.; Khan, Z.A. Effect of Alloying and Reinforcing Nanocomposites on the Mechanical, Tribological, and Wettability Properties of Pulse-Electrodeposited Ni Coatings. *Micromachines* **2025**, *16*, 175. <https://doi.org/10.3390/mi16020175>

Copyright: © 2025 by the authors. Licensee MDPI, Basel, Switzerland. This article is an open access article distributed under the terms and conditions of the Creative Commons Attribution (CC BY) license (<https://creativecommons.org/licenses/by/4.0/>).

Keywords: tribology; pulse electrodeposition coating; nanocomposites; wettability; nanotribology; nanohardness; contact angle

1. Introduction

The electrodeposition of metals and alloys on various metallic substrates is widely applied in different domains, including aerospace, mechanical, electrical, automotive, and nuclear industries [1–3]. A new era of composites has begun, with finely dispersed nanoparticles being electrochemically deposited within a metallic matrix. Bespoke coating characteristics are achieved by customising electroplating physical properties, types of nano constituents and electrolytic characteristics and are key benefits of electroless pulse coating techniques. Other advantages include low working temperatures, ease of maintenance, and cost-effectiveness [4–10].

On account of their strong resistance to thermal oxidation and corrosion, Ni coatings have gained much attention. The use of W, Mo, Mn, Cr, and P nano constituents as additives to Ni-based coatings leads to significant tribo performance. Further improvements can be achieved with the addition of reinforcing nanocomposites to the Ni metal matrix [6,11–24]. Ni-Co alloy nanocomposite coatings' magnetic, catalytic, electrochemical energy storage

capacity, high-temperature resistant oxidation (including corrosion), and anti-wear properties are desirable across various industries, including sensors, automotive components, actuators, inductors, aerospace technologies, and supercapacitors [25–29].

The incorporation of nanoparticles into a metal matrix (MMC) through pulse electrodeposition improves the tribological properties of these nanocomposite coatings. MMC variations during the process lead to the optimisation of nanocoatings' morphological, structural, mechanical, and tribo properties. The influence of Al₂O₃ in Ni coatings has been studied by Chen et al. in terms of variation in frequency, which affects the volumetric change in Al₂O₃ deposition [30]. An inverse relation between frequency and hardness has been observed. A resultant microstructure variation leads to abrasive wear mode as the key tribo failure mechanism. The addition of Al₂O₃ to a coating restricts grain movement, which results in an improvement in overall hardness [4,31,32]. Alumina's addition has led to enhanced wear resistance due to hardness improvement. The addition of Al₂O₃ results in an increase in ductility and, in turn, deformation hardening and resistance, ensuring increased load bearing and wear resistance capacities (Gul et al.) [31]. The addition of alumina was seen to restrict grain growth, which reduces the grain size, leading to an increase in hardness. This mechanism enhanced the tribological properties of nanocomposite coatings [33]. Similar observations were made regarding the hardness of nanocoatings with SiC and ZrO₂. The addition of these secondary nanocomposites improved the hardness [6,9,34–37]. Gyftou et al. [35] noticed a decrease in grain size when SiC particles were added. SiC particles demonstrated a higher resistance to wear in coatings due to a similar inverse relation between hardness and frequency, observing an increase to decrease and vice versa. Zhou et al. [9] observed a pore-free, uniform thickness, and defect-free Ni coating with SiC as a reinforcing nanocomposite. Mostafa et al. [36] reported a nodular microstructure for NiP-ZrO₂ coatings, which helps improve the hardness of coatings.

There have been several research on the variation of physical parameters of Ni pulse electrodeposition coating. Investigation of synergistic effects of alloying element (Co), with various reinforcing MMCs (Al₂O₃, SiC, and ZrO₂). Ni-Co exhibits a unique magnetic property, is a novel approach, which makes it a potential candidate in the electronics industry. The reinforcing MMCs are selected due to their extensive application in mechanical, aerospace and automobile industries. This comprehensive analysis uniquely evaluates structural, mechanical, tribological, and wettability properties, targeting multifunctional applications across the electronics, aerospace, and automotive industries.

2. Materials and Methods

Pulse electrodeposition was selected to prepare the composite coating. EN1A was selected as the cathode and nickel plate as the anode, with the cathode being the target material wherein the coating is formed. EN1A steel was selected as the substrate due to its low cost, handiness, and adhesive properties. EN1A was produced as a circular-shaped cathode with a diameter × thickness of 30 mm × 3.5 mm. The following Table 1 provides chemical composition information. The nickel anode was produced in a rectangular shape of 2 mm thickness. Surface conditioning was conducted by using emery paper and water lubrication to obtain a surface areal roughness below 0.05 μm. Furthermore, samples were conditioned ultrasonically with distilled water and acetone to eliminate oxide layers and contaminants present on the surface.

Table 1. Chemical composition of EN1A steel substrate.

C	Si	Mn	P	S
0.09	0.25	0.91	0.71	0.5

A modified Watt solution was employed as the electrolyte for the present pulsed electrodeposition coating. For the Ni-Co coating, cobalt sulphate was added to the modified Watt solution as the cobalt source. Aluminium oxide, silicon carbide, and zirconium dioxide were added to the Ni-Co solution as reinforcing MMCs (Figure 1). Nickel sulphate, nickel chloride, boric acid, and cobalt sulphate were purchased from Thermo Scientific (Waltham, MA, USA), Acros Organics (Geel, Belgium), Fisher Scientific (Pittsburgh, PA, USA), and Alfa Aesar (Lancashire, UK), respectively. Aluminium oxide and zirconium dioxide were obtained from Aldrich Chemistry (Dorset, UK) and silicon carbide was obtained from Io-Li-Tec (Heilbronn, Germany). Chemicals were in crystal form with 98% purity. A different electrolyte was prepared for each reinforcing material. The electrolytes were stirred with a magnetic stirrer for 24 hrs and further ultrasonication of 10 kHz was provided for 20 mins before initiating the coating process. The composition of electrolytes is given in Table 2.

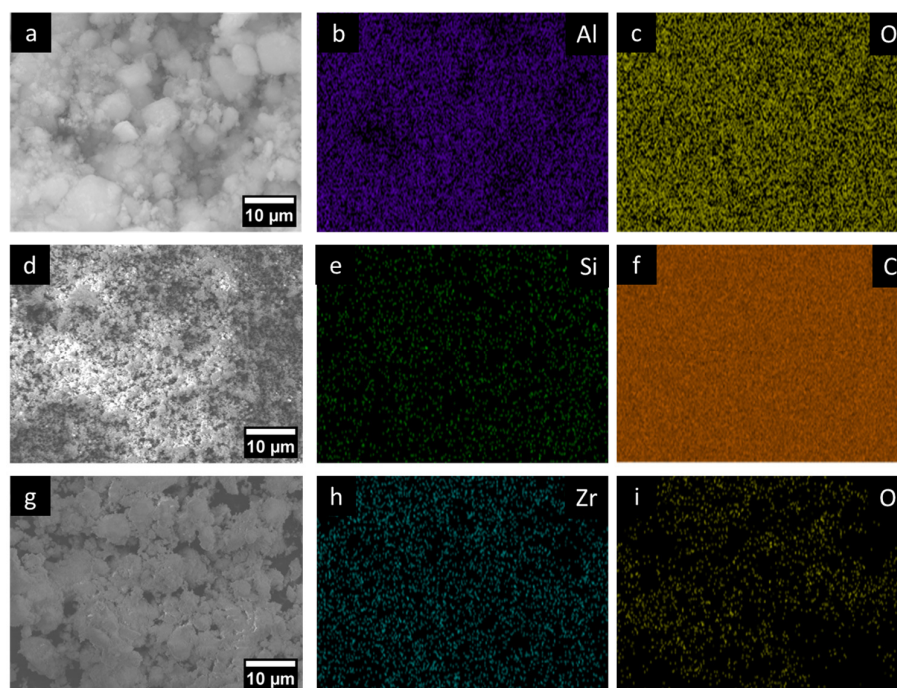


Figure 1. SEM images of MMCs used. (a) Al_2O_3 (d) SiC, and (g) ZrO_2 with their corresponding elemental map, {(b,c) Al_2O_3 (e,f) SiC and (h,i) ZrO_2 }.

Table 2. Electrolyte composition.

Chemical Constituent	Concentration (g/L)	Property
Nickel Sulphate ($\text{NiSO}_4 \cdot 6\text{H}_2\text{O}$)	265	Watts Solution/Nickel Source
Nickel Chloride ($\text{NiCl}_2 \cdot 6\text{H}_2\text{O}$)	48	
Boric Acid (H_3BO_3)	31	
Cobalt Sulphate ($\text{CoSO}_4 \cdot 6\text{H}_2\text{O}$)	40	Cobalt Source
Aluminium Oxide (Al_2O_3)	10	Al_2O_3 Source
Silicon Carbide (SiC)	10	SiC Source
Zirconium Dioxide (ZrO_2)	10	ZrO_2 Source

A pulse power generator was employed for the current coating. The duty cycle, current density, and frequency were kept constant with those values from earlier studies [38–40]. A constant duty cycle of 20% ($T_{\text{ON}} = 20$ ms and $T_{\text{OFF}} = 80$ ms) and current density and frequency at $3 \text{ A}/\text{dm}^2$ and 10 Hz, respectively, were maintained. Constant stirring of the electrolytes was employed during the coating process. A 300 rpm speed was set to facilitate

the stirring process, which ensured the turbulent flow of chemicals throughout the coating process. The temperature of the electrolyte was 60 ± 5 °C and the electrolyte pH was 4.2 ± 0.2 . The time of coating was set to 60 min. The test configuration is shown in Table 3. Post-electrodeposition, samples were rinsed in an ultrasonic bath containing distilled water and acetone to eliminate residual contaminants. Samples were cleansed in a controlled lab environment.

Table 3. Pulse electrodeposition coating conditions.

Condition	Parameter
Current Density (A/dm ²)	3
Duty Cycle (%)	20
Time (min)	60
Temperature (°C)	60
Stir Speed (rpm)	300
pH	4.2 ± 0.2
Cathode	EN1A
Anode	Nickel Plate

2.1. Characterisation of Nanocrystalline Coating

A Scanning Electron Microscope (SEM) (JEOL, Garden City, UK) was deployed for surface analysis. Nanocrystalline coatings' constituents were measured by Energy Dispersive X-ray (EDS) (Oxford Instruments, Abingdon, UK) coupled with the SEM.

Samples' roughness was analysed by utilising White Light Interferometry; the parameters of Ra , Rq , Rt and Rz were obtained along with bearing area curves. Ra can be defined as "the arithmetic mean deviation of the sampling length, whereas Sa is defined as the arithmetic mean deviation of the sampling area". Rq is defined as "the root mean square deviation of the assessed sampling length" and Sq is "the root mean square deviation of the assessed sampling area". Rt and St are "the total height of the profile (height between deepest valley and highest peak) of the assessed sampling length and sampling area", respectively. Rz is "the maximum height of the profile in the sampling length".

$$Ra = \frac{1}{L} \int |z(x)| dx$$

$$Sa = \frac{1}{A} \iint |z(x, y)| dx dy$$

where ' L ' is sampling length, ' A ' is sampling area, and z is the ordinate of the profile curve at a given ordinate or height (x, y) [41–43].

2.2. Mechanical Characterisation

A 3-faced Berkovich, pyramidal diamond indenter was employed to acquire nanohardness data of coatings (Micromaterials, Wrexham, UK). A total of 15 indents were made on the coating and the values were analysed to determine nanohardness and reduced modulus.

Tribological experiments were conducted using a modified ball-on-plate reciprocating tribometer. Here, 6 mm diameter AISI 52100 chrome steel balls served as the counter face against the coated flat samples. The coated samples were secured within a stationary specimen chamber, while the counter face underwent reciprocating motion at a frequency of 5 Hz. Key experimental parameters were maintained at constant values throughout: a contact load of 2 N, 2000 cycles, a sliding distance of 2 m, and a frequency of 5 Hz. The experiments were conducted in ambient room temperature conditions. Post tribological experiments, wear volume was obtained with the help of a profilometer. The roughness

of the wear scar was obtained and analysed. The scars were analysed under SEM to understand the wear mechanisms involved.

To investigate tribological behaviour at the nanoscale, nanotribological wear experiments were performed on the coatings. A spherical indenter with a 28 μm diameter was employed for multi-wear analysis. Three distinct loads were applied: 100 mN, 200 mN, and 300 mN. A total of 12 passes were executed along a 1000 μm track at a scan velocity of 10 $\mu\text{m/s}$. The initial and final passes served as topography scans, conducted at a minimal load of 0.5 mN. Load application commenced at a distance of 200 μm from the scan initiation point at a loading rate of 4 mN/s. To ensure repeatability, each load condition was replicated three times. Wear depth and scar roughness were subsequently quantified using a profilometer to analyse the nanotribology scars. Scanning electron microscopy (SEM) was utilised for further examination of wear scars' morphology.

To study the wettability properties of the coatings, they were subjected to wettability analysis. A custom-made setup was used for the wettability analysis, with a droplet size of 7 μL . A DSLR camera was used to capture images of the droplet size, and images were analysed with ImageJ (1.54 g), an open licenced software.

3. Results

3.1. Surface Morphology

The Ni pulse electrodeposition coating with Co as the alloying particle with Al_2O_3 , SiC, and ZrO_2 as reinforcing nanocomposites is illustrated in Figure 2. A fine grain structure was observed for Ni-coated surfaces. A globular grain structure was detected for the Ni coating with a 0.55 μm average grain size. The addition of Co particles as the alloying element caused the grain size to decrease to 0.36 μm . A further decrease in grain size could be observed when reinforcing nanoparticles were introduced. With the addition of Al_2O_3 , SiC, and ZrO_2 as the reinforcing agents, the grain size further decreased to 0.37 μm , 0.51 μm , and 0.31 μm , respectively. Incorporating alloying and reinforcing MMCs into Ni coatings resulted in a notable reduction in grain size, ranging from ~7% to ~43%. There are several explanations for why adding alloying element and MMCs causes the grain size to decrease. Firstly, the presence of Co as an alloying element resulted in increased nucleation sites. An increase in nucleation regions yielded decreased grain size and grain growth [44,45]. Increasing the pulse-off duration facilitated greater replenishment of alloying elements and metallic matrix composites (MMCs) in the vicinity of the substrate. Subsequently, during the pulse-on phase, these replenished nanoparticles were more readily adsorbed onto the substrate. This enhanced adsorption resulted in an increased density of nucleation sites and consequently a reduction in the overall grain size. It was espied earlier that with a decrease in duty cycle, a finer but more compact grain structure can be obtained [46–48]. The influence of grain size on nanohardness and nanotribological properties is explored.

The mechanism of the particle co-deposition of Co and MMCs can be explained with Guglielmi's model. The Guglielmi model describes the transfer mechanism of nanoparticles from an electrolytic solution to a substrate, forming a composite coating. According to this model, the process involves two key stages: loose adsorption, where the particles are loosely adsorbed to the cathode surface by Van der Waals forces, and strong adsorption, where under the electric field and electrochemical reactions, the particles transition to the strong adsorption state [49,50].

To understand the elemental configuration associated with the nanocomposite coating, EDS analyses were obtained. Figure 3 depicts the coatings' EDS mapping. For the nickel coating, the coating consisted of only Ni, which was 100%. The amount of Ni decreased when Co was added as an alloying element, to 57%, and the remainder was Co, 43%. A further decrease could be observed with the addition of reinforcing agents. When Al_2O_3

was added to the coating as an MMC, the Ni and Co presence decreased to 55% and 40%, respectively, with 5% Al_2O_3 . Ni-Co/SiC and Ni-Co/ ZrO_2 had similar decreases in Ni and Co content. Ni-Co/SiC had 58% of Ni and 35% of Co, with SiC having 7%. Ni-Co/ ZrO_2 also exhibited a similar decline in Ni and Co, 54% and 41%, respectively, with ZrO_2 5%.

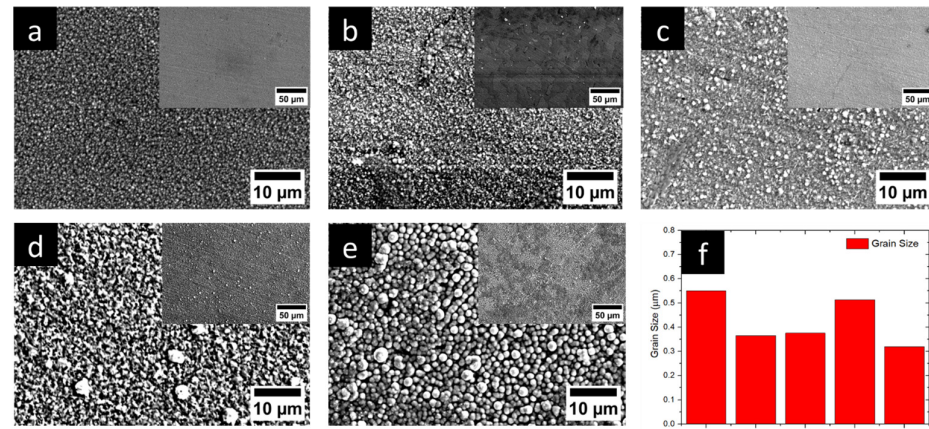


Figure 2. SEM micrographs of the coatings (with low magnification in the inset image): (a) Ni, (b) Ni-Co, (c) Ni-Co/ Al_2O_3 , (d) Ni-Co/SiC, (e) Ni-Co/ ZrO_2 , (f) grain size.

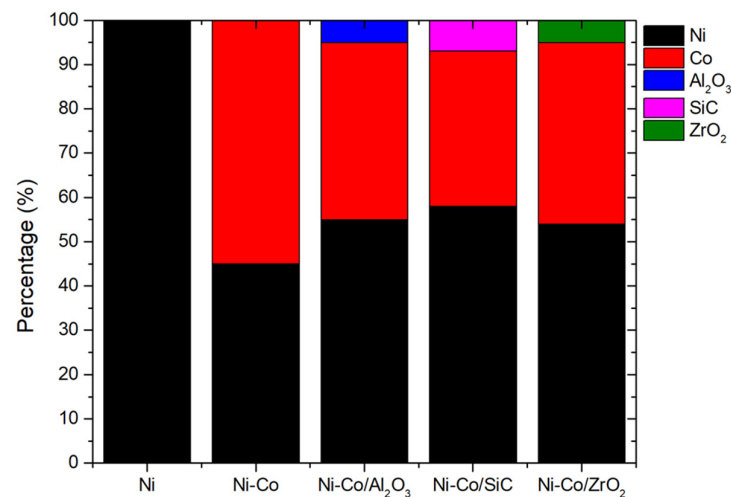


Figure 3. EDS analysis of pulsed electrodeposition coatings of Ni, Ni-Co alloy, and Ni-Co alloy with reinforced materials (Ni-Co/ Al_2O_3 , Ni-Co/SiC, and Ni-Co/ ZrO_2).

3.2. Surface Roughness

Profilometer images of the coatings are shown in Figure 4. Line roughness parameters, including R_a , R_q , R_z , and R_t , were evaluated for the nanocrystalline coatings and are presented in Figure 5. The Ni-coating exhibited a line roughness of 0.122 μm. Roughness values for Ni-Co, Ni-Co/ Al_2O_3 , Ni-Co/SiC, and Ni-Co/ ZrO_2 were determined to be 0.105 μm, 0.158 μm, 0.096 μm, and 0.102 μm, respectively.

To gain a more precise understanding of line roughness, the root-mean-square (RMS) line roughness was calculated, revealing a trend consistent with the overall line roughness. Ni-Co/ Al_2O_3 exhibited the highest RMS roughness at 0.230 μm, followed by Ni, Ni-Co, Ni-Co/SiC, and Ni-Co/ ZrO_2 with RMS values of 0.168 μm, 0.151 μm, 0.143 μm, and 0.130 μm, respectively.

Maximum peak-to-valley height (R_t) was measured as 1.447 μm, 1.628 μm, 1.694 μm, 1.517 μm, and 1.184 μm for Ni, Ni-Co, Ni-Co/ Al_2O_3 , Ni-Co/SiC, and Ni-Co/ ZrO_2 , respectively. Similarly, R_z values were obtained, displaying a trend analogous to the RMS

line roughness. R_z values were recorded as 1.258 μm , 1.079 μm , 1.368 μm , 0.959 μm , and 0.859 μm , respectively.

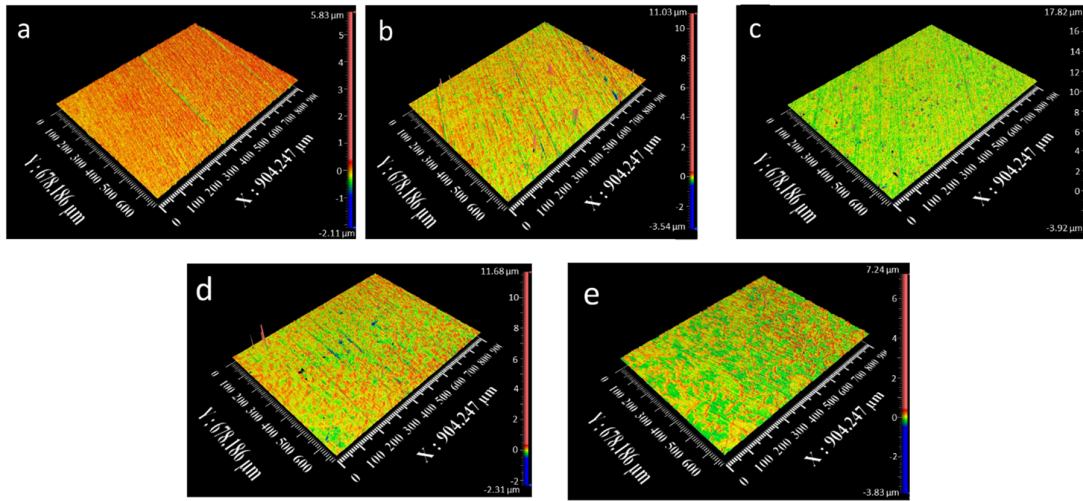


Figure 4. Surface profiles of (a) Ni, (b) Ni-Co, (c) Ni-Co/ Al_2O_3 , (d) Ni-Co/SiC, and (e) Ni-Co/ ZrO_2 .

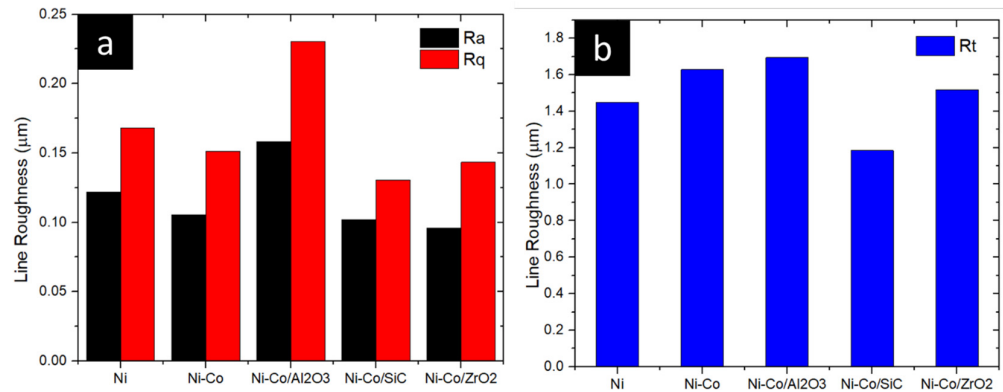


Figure 5. Line roughness of pulse electrodeposition coating. (a) Ra and Rq (b) Rt.

To gain a comprehensive understanding of surface roughness, areal roughness analysis was conducted, providing a two-dimensional assessment of surface topography, as depicted in Figure 6. The areal roughness of the Ni coating was measured at 0.124 μm , which subsequently varied to 0.108 μm , 0.162 μm , 0.104 μm , and 0.103 μm for Ni-Co, Ni-Co/ Al_2O_3 , Ni-Co/SiC, and Ni-Co/ ZrO_2 , respectively.

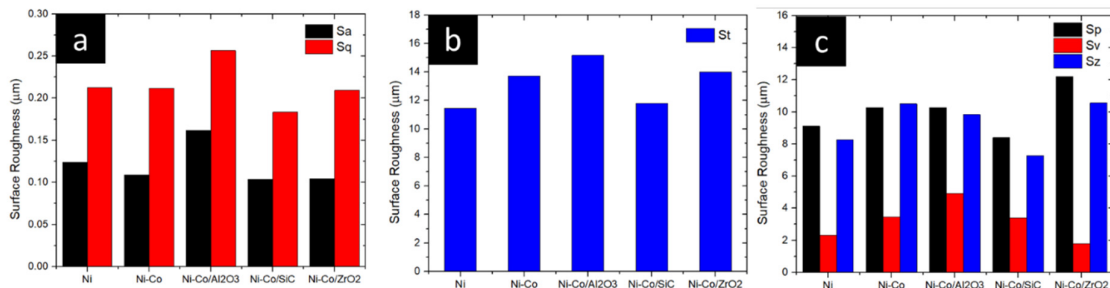


Figure 6. Surface roughness of pulse electrodeposition coatings. (a) Sa and Sq, (b) St and (c) Sp, Sv, Sz.

Consistent with previous observations, the root-mean-square (Sq) roughness was also evaluated to provide a more in-depth analysis of surface texture. Sq values were recorded as 0.212 μm , 0.211 μm , 0.256 μm , 0.209 μm , and 0.183 μm , respectively. The incorporation of alloying elements and reinforcing nanocomposites into the Ni coating significantly altered the surface morphology.

Maximum peak-to-valley height of the entire surface, denoted as St , was also considered. St values were observed to be 11.456 μm , 13.720 μm , 15.175 μm , 14.006 μm , and 11.797 μm , respectively. In line with the observed surface roughness trends, an increase in St was noted for the coatings incorporating reinforcing and alloying agents.

To determine average distance between peaks and valleys, average peak-to-valley height (Sz) was analysed. Sz values were found to be 8.27 μm , 10.49 μm , 9.83 μm , 10.55 μm , and 7.27 μm , respectively.

The bearing area curves of the nanocomposite coatings were analysed and are shown in Figure 7. It is seen that the Rk value was highest for Ni and was almost similar to Ni-Co/ Al_2O_3 . Following that, all the nanocoating MMCs had a lower Rk value. The Rk value signifies the core roughness depth over the sampling area. The Rk value was efficacious over the tribological properties of the coating, which is discussed in later sections. The MR1 and MR2 values were analysed from the bearing area curves of the nanocomposite coatings. It was observed that MR1 values were similar for all the nanocomposite coatings. However, while analysing MR2, Ni and Ni-Co/ Al_2O_3 had lower values and all other coatings had a higher MR2 value. The influence of bearing area curve and roughness on nanotribological properties is explored further with a nanotribometer.

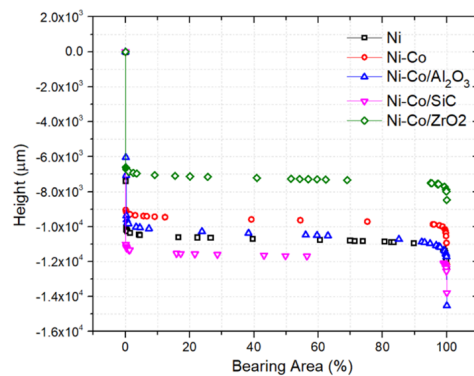


Figure 7. Bearing area curves of pulse electrodeposition coatings.

3.3. Nanohardness

Nanoindentation tests were conducted to investigate nanocoatings’ mechanical properties. Figure 8 illustrates the influence of alloying and reinforcing nanoparticles on nanohardness. The Ni coating exhibited a hardness of 3.51 GPa. Subsequently, an increase in nanohardness was observed in Ni-Co, Ni-Co/ Al_2O_3 , Ni-Co/SiC, and Ni-Co/ ZrO_2 , attributed to the presence of reinforcing nanomaterials.

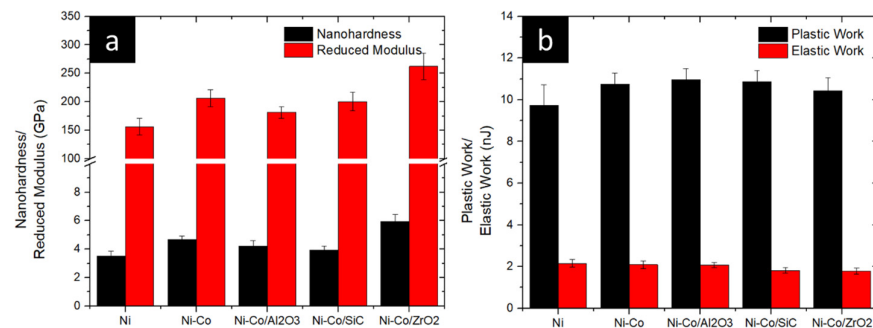


Figure 8. Effect of alloying and reinforcing composites of Ni coating on (a) nanohardness and reduced modulus and (b) plastic–elastic work.

The highest hardness, 5.95 GPa, was achieved for the Ni-Co/ ZrO_2 coating, where ZrO_2 served as the reinforcing agent. This represents a substantial 66.51% enhancement

compared to the base Ni coating. Conversely, the lowest hardness, 3.93 GPa, was observed for the SiC-reinforced coating.

The nanohardness of Ni-Co and Ni-Co/Al₂O₃ was determined to be 4.69 GPa and 4.22 GPa, respectively. The incorporation of Co into the Ni matrix resulted in a 33.61% increase in nanohardness compared to the pristine Ni coating.

In conclusion, the addition of alloying elements and reinforcing nanocomposites to the Ni coating led to a notable enhancement in hardness, ranging from approximately 11% to 69%.

In addition to the above, the reduced modulus of the Ni-based nanocomposite coating was also obtained. The reduced modulus of the pure Ni coating was 156.32 GPa, which was the lowest among all the coatings. The reduced modulus of Ni-Co with alloying reagent was 206.13 GPa and with the additions of reinforcing composites Ni-Co/Al₂O₃, Ni-Co/SiC and Ni-Co/ZrO₂ having reduced moduli of 181.51 GPa, 200.25 GPa, and 262.24 GPa, respectively. With the addition of reinforcing and alloying coating chemicals, the reduced modulus changed.

The hardness of metal matrix composites is influenced primarily by grain refining, dispersion strengthening, and the hardness of the metal matrix. With the addition of Co, nucleation sites increased, which caused an increase in grains, resulting in a decrease in grain size. A refined grain size will hinder the movement of grains, which will increase hardness. A further change in nanohardness was observed with the addition of reinforcing nanocomposites. The metal matrix deposited can influence the hardness in two ways. Firstly, by dispersion strengthening, the alloying elements and MMCs present in the coating will hinder the movement of the grains. This hindered movement will cause an increase in hardness. Secondly, the hardness of incorporated MMCs will influence the hardness of the coating. In the present study, Al₂O₃, SiC, and ZrO₂ were the reinforcing MMCs. The hardness of reinforcing MMC particles will increase the hardness of the overall coating surface. Therefore, the synergistic effect of reduced grain size and hardness of the reinforcing particles will increase the hardness of the coatings. The influence of nanohardness on the tribological properties of coatings is explored with a nanotribometer and ball-on-plate tribometer.

3.4. Sliding Wear Behaviour

The wear volume of coatings is shown in Figure 9. The pure Ni coating had a wear volume of $6.38 \times 10^{15} \text{ nm}^3$, which was followed by Ni-Co/SiC having a wear rate of $4.70 \times 10^{15} \text{ nm}^3$. Ni-Co/ZrO₂ and Ni-Co had wear rates of $4.00 \times 10^{15} \text{ nm}^3$ and $3.69 \times 10^{15} \text{ nm}^3$, respectively, followed by Ni-Co/Al₂O₃, which had the best wear rate of $3.16 \times 10^{15} \text{ nm}^3$. Therefore, it can be concluded that Ni-Co/Al₂O₃ had the lowest wear rate of $3.16 \times 10^{15} \text{ nm}^3$, which had Al₂O₃ as the reinforcing agent. The coating with the least wear resistance was the Ni coating. The addition of Co to Ni was seen to improve the wear properties. The reinforcing agents Al₂O₃, SiC, and ZrO₂ helped in increasing the wear resistance of the coating.

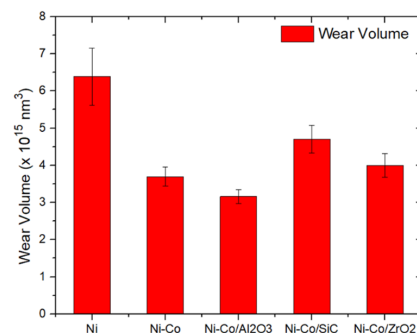


Figure 9. Effect of alloying and reinforcing composites of Ni coating over tribological properties.

Ni-Co/ Al_2O_3 having the highest wear resistance is due to Al_2O_3 which acts as a lubricant. After the initial cycles, Al_2O_3 detached from the coating surface, which acted as a lubricant. Three-body interaction was initiated, with Al_2O_3 acting as a lubricant. SiC also exhibited similar properties, with a decreased wear rate. However, the lower hardness of Ni-Co/SiC resulted in the removal of the coating layer at a higher rate, resulting in a higher wear rate when compared to Ni-Co/ Al_2O_3 . Ni-Co/ ZrO_2 , which had ZrO_2 as the reinforcing agent, was also seen to have higher wear resistance. ZrO_2 is known to have higher hardness by itself, which helped in improving the wear rate.

SEM images of wear scars were obtained and are provided in Figure 10 to understand prevailing wear mechanisms. Abrasive wear and oxidation wear were seen, along with delamination and adhesive wear in the case of coatings. The pitting of nanoparticles was also observed on wear tracks. With the Ni-Co coating, abrasive wear along with microploughing and delamination wear was observed. For the Ni-Co/ Al_2O_3 coating, delamination wear was dominant along with microploughing and abrasion. However, in Ni-Co/SiC, oxidation wear was the predominant mechanism, with micropitting and delamination also present. Similar observations were observed in Ni-Co/ ZrO_2 as well. These findings are consistent with previous research, demonstrating alignment with earlier studies. Therefore, it can be concluded that alloying and reinforcing elements improved the tribological attributes of Ni composite coatings.

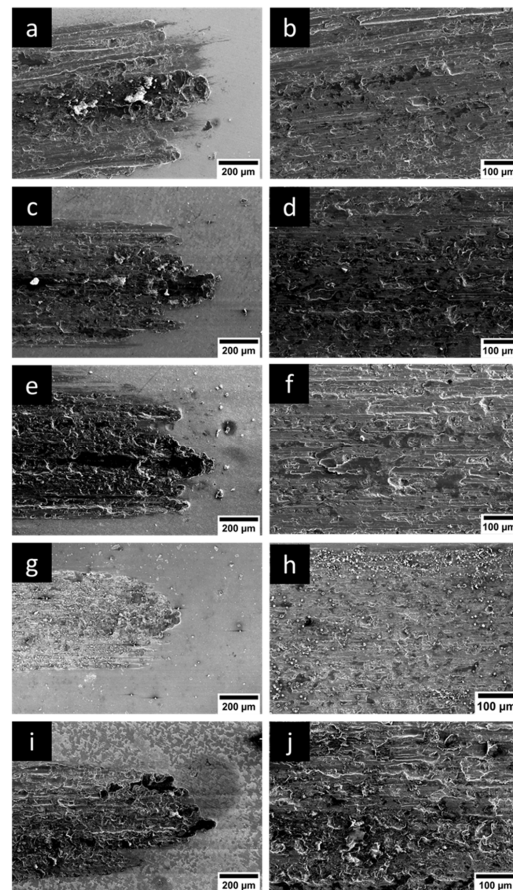


Figure 10. Wear morphologies of Ni nanocomposites with different alloying and reinforcing composites. (a,c,e,g,i) Wear morphology at edges and (b,d,f,h,j) wear morphology and centre of wear scar. (a,b) Ni, (c,d) Ni-Co, (e,f) Ni-Co/ Al_2O_3 , (g,h) Ni-Co/SiC, (i,j) Ni-Co/ ZrO_2 .

3.5. Nanotribology Analysis

The nanotribological analysis was performed to gain a deeper understanding of the tribological properties on a nano-level load. The load was varied from 100 mN to

300 mN and wear volume was analysed. The wear volumes of various nanocomposite coatings are displayed in Figure 11, with SEM images of wear scars in Figure 12. At the load of 100 mN, Ni-Co/SiC exhibited the best wear properties with a wear volume of $1.71 \times 10^{-3} \text{ mm}^3$, which was accompanied by Ni-Co/ZrO₂, Ni-Co/Al₂O₃, Ni-Co, and Ni, with a wear volume of $2.78 \times 10^{-3} \text{ mm}^3$, $2.89 \times 10^{-3} \text{ mm}^3$, $3.26 \times 10^{-3} \text{ mm}^3$, and $4.81 \times 10^{-3} \text{ mm}^3$. When the load was increased to 200 mN, Ni-Co/ZrO₂ had a wear volume of $4.50 \times 10^{-3} \text{ mm}^3$, which was followed by Ni-Co/SiC, Ni-Co/Al₂O₃, Ni-Co, and Ni with a wear volume of $5.04 \times 10^{-3} \text{ mm}^3$, $5.24 \times 10^{-3} \text{ mm}^3$, $5.30 \times 10^{-3} \text{ mm}^3$, and $5.63 \times 10^{-3} \text{ mm}^3$. Furthermore, when load was increased to 300 mN, the wear volume was best for Ni-Co/Al₂O₃, which was followed by Ni-Co/SiC, Ni-Co/ZrO₂, Ni-Co, and Ni with a wear volume of $7.02 \times 10^{-3} \text{ mm}^3$, $7.98 \times 10^{-3} \text{ mm}^3$, $7.46 \times 10^{-3} \text{ mm}^3$, $7.57 \times 10^{-3} \text{ mm}^3$, and $7.72 \times 10^{-3} \text{ mm}^3$, respectively. It can be espied from the analysis that during all the loads, the nanocoating with reinforcing nanocomposites had nanowear superior to that of the Ni and Ni-Co coatings.

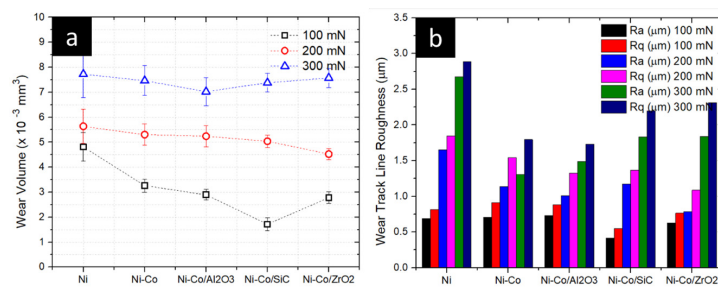


Figure 11. Effect of alloying and reinforcing composites of Ni coating over (a) nanotribological properties, (b) wear line roughness.

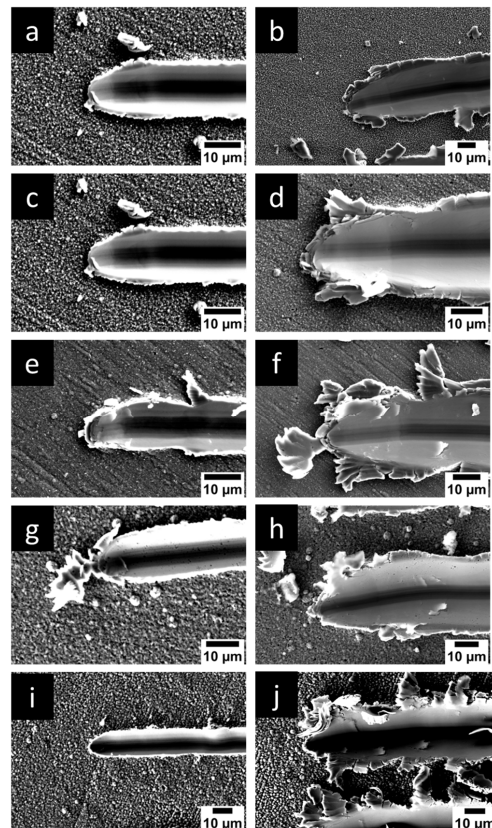


Figure 12. Nanowear morphologies of Ni nanocomposites with different alloying and reinforcing composites. (a,c,e,g,i) Wear morphology at edges and (b,d,f,h,j) wear morphology and centre of wear scar. (a,b) Ni, (c,d) Ni-Co, (e,f) Ni-Co/Al₂O₃, (g,h) Ni-Co/SiC, (i,j) Ni-Co/ZrO₂.

By classical Archard's law,

$$Q \propto \frac{WL}{H}$$

The wear volume (Q) is governed by the equation $Q \propto W*L/H$, where W = total normal load, L = sliding distance, and H = hardness of contacting surface. This equation reveals an inverse relationship between wear volume and surface hardness. Nanocomposite coatings, such as Ni coatings incorporating alloying and reinforcing agents, exhibit enhanced hardness. This increased hardness translates to a reduced wear rate for the nanocoating. Notably, the addition of reinforcing agents to Ni-Co coatings has been observed to significantly improve their tribological properties.

Surface roughness significantly influences the wear rate of coatings. The incorporation of alloying and reinforcing agents into pure Ni coatings often results in increased surface roughness, characterised by the presence of more pronounced peaks. During initial tribological interactions, these peaks engage with the counter-surface, leading to localised high-contact pressures. This elevated pressure can accelerate material removal. Conversely, smoother surfaces with lower roughness exhibit a larger contact area, distributing the load more evenly and consequently reducing contact pressure. This diminished pressure translates to a lower rate of material removal. Therefore, the synergistic effect of enhanced nanohardness and optimised surface roughness is crucial in achieving superior wear resistance in these coatings.

3.6. Wettability

Contact angles of nanocomposite coatings were measured with a customised setup camera, and the images were analysed with ImageJ, an open licence software. The correlation between the hydrophilic properties of various nanocomposite coatings was analysed (Figure 13). The hydrophilic properties were exhibited by all the nanocomposite coatings. Ni-Co/ Al_2O_3 had the best hydrophilic property among all the composite coatings with a contact angle of 64.32° . This was followed by Ni and Ni-Co/ Al_2O_3 with a contact angle of 66.53° and 74.30° , respectively. However, Ni-Co and Ni-Co/ ZrO_2 had almost similar hydrophilic properties with a contact angle of 85.50° and 85.43° , respectively.

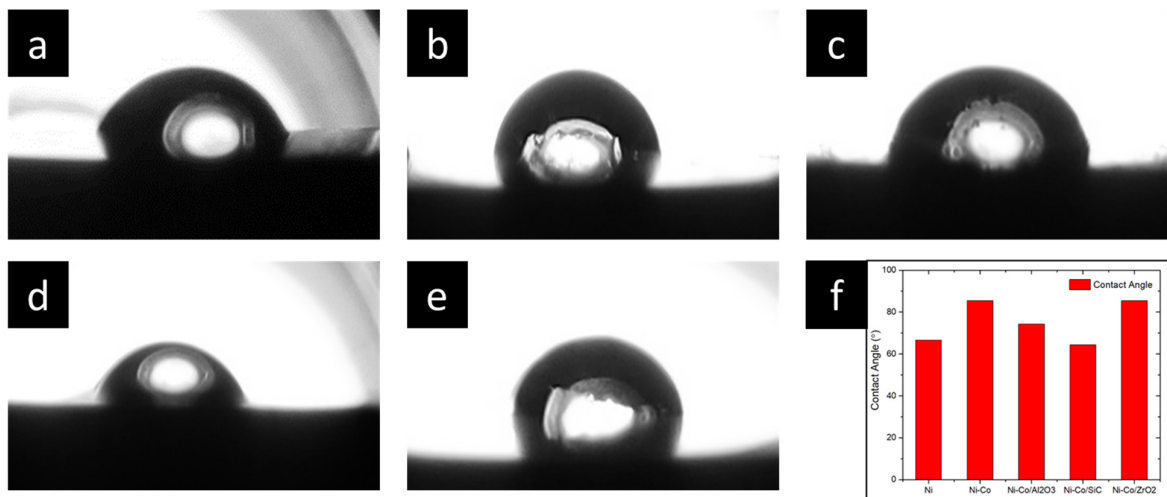


Figure 13. Effect of alloying and reinforcing composites of Ni coating over contact angle properties. (a) Ni, (b) Ni-Co, (c) Ni-Co/ Al_2O_3 , (d) Ni-Co/SiC, (e) Ni-Co/ ZrO_2 , (f) comparisons.

Based on the findings from contact angle measurements, it is evident that the nanocomposite coatings exhibited hydrophilic properties. Traditionally, surface roughness is a key factor influencing contact angle properties, as elucidated by Cassie–Baxter and Wenzel theories. However, contrary to expectations, the roughness in this study did not signifi-

cantly impact the contact angle properties of the coating. Instead, the dominant influence stemmed from the surface energy of the nanoparticles and nanocomposites. Notably, metals are known to possess higher surface energy, and this characteristic was effectively transferred to the coating material. Consequently, all the pulse electrodeposited coatings in this study demonstrated hydrophilic properties.

4. Conclusions

The pulse electrodeposition of Ni coatings, with Co as an alloying element and reinforced by Al₂O₃, SiC, and ZrO₂ nanomaterials, was successfully performed. The process exhibited a synergistic effect between the alloying element and reinforcing nanocomposites, significantly enhancing the coating properties. The following conclusions were made:

- Grain size reduction of ~7%–~43% with the incorporation of alloying and reinforcing nanocomposites.
- Improved surface characteristics, as evidenced by surface roughness and bearing area curve analyses.
- Enhanced coating hardness, with increases of ~11%–~69% when compared with the Ni coating, and with Ni-Co/ZrO₂ achieving the highest hardness of 5.95 GPa.
- Superior wear resistance, with Ni-Co/Al₂O₃ demonstrating a ~51% improvement over pure Ni coatings.
- Tribological property enhancements, with improvements ranging from ~2% to ~65%, confirmed through nanotribological assessments.
- Hydrophilic behaviour in all coatings, with Ni-Co/ZrO₂ exhibiting the highest contact angle and Ni-Co/SiC, the lowest.

Author Contributions: Conceptualisation, A.J. and Z.A.K.; methodology, A.J.; software, Z.A.K.; validation, A.J. and Z.A.K.; formal analysis, A.J.; investigation, A.J.; resources, Z.A.K.; data curation, A.J. and Z.A.K.; writing—original draft preparation, A.J.; writing—review and editing, A.J., A.S. and Z.A.K.; visualisation, A.J.; supervision, A.S. and Z.A.K.; project administration, A.S. and Z.A.K.; funding acquisition, Z.A.K. and A.S. All authors have read and agreed to the published version of the manuscript.

Funding: This research was funded by ASMPT SMT Solutions, Grant No. 12285 for conducting this research.

Data Availability Statement: All relevant data is included in this paper.

Acknowledgments: The authors would like to acknowledge in kind support by ASMPT SMT Solutions to conduct this research.

Conflicts of Interest: The authors declare no conflicts of interest.

References

1. Peng, B.Y.; Nie, X.; Chen, Y. Effects of Surface Coating Preparation and Sliding Modes on Titanium Oxide Coated Titanium Alloy for Aerospace Applications. *Int. J. Aerosp. Eng.* **2014**, *2014*, 64036. [[CrossRef](#)]
2. Baptista, A.; Silva FJ, G.; Porteiro, J.; Míguez, J.L.; Pinto, G.; Fernandes, L. On the Physical Vapour Deposition (PVD): Evolution of Magnetron Sputtering Processes for Industrial Applications. *Procedia Manuf.* **2018**, *17*, 746–757. [[CrossRef](#)]
3. Chen, H.; Wang, X.; Zhang, R. Application and Development Progress of Cr-Based Surface Coatings in Nuclear Fuel Element: I. Selection, Preparation, and Characteristics of Coating Materials. *Coatings* **2020**, *10*, 808. [[CrossRef](#)]
4. Wang, W.; Hou, F.Y.; Wang, H.; Guo, H.T. Fabrication and Characterization of Ni-ZrO₂ Composite Nano-Coatings by Pulse Electrodeposition. *Scr. Mater.* **2005**, *53*, 613–618. [[CrossRef](#)]
5. Lajevardi, S.A.; Shahrabi, T. Effects of Pulse Electrodeposition Parameters on the Properties of Ni-TiO₂ Nanocomposite Coatings. *Appl. Surf. Sci.* **2010**, *256*, 6775–6781. [[CrossRef](#)]

6. Wasekar, N.P.; Bathini, L.; Ramakrishna, L.; Rao, D.S.; Padmanabham, G. Pulsed Electrodeposition, Mechanical Properties and Wear Mechanism in Ni-W/SiC Nanocomposite Coatings Used for Automotive Applications. *Appl. Surf. Sci.* **2020**, *527*, 146896. [[CrossRef](#)]
7. Song, R.; Zhang, S.; He, Y.; Li, H.; Fan, Y.; He, T.; Zhang, Y.; Xiang, Y.; Zhang, H. Effect of H-MWCNTs Addition on Anti-Corrosion Performance and Mechanical Character of Ni-Cu/H-MWCNTs Composite Coatings Prepared by Pulse Electrodeposition Technique. *Colloids Surf. A Physicochem. Eng. Asp.* **2021**, *630*, 127519. [[CrossRef](#)]
8. Xia, F.; Li, C.; Ma, C.; Li, Q.; Xing, H. Effect of Pulse Current Density on Microstructure and Wear Property of Ni-TiN Nanocoatings Deposited via Pulse Electrodeposition. *Appl. Surf. Sci.* **2021**, *538*, 148139. [[CrossRef](#)]
9. Zhou, Y.; Xie, F.Q.; Wu, X.Q.; Zhao, W.D.; Chen, X. A Novel Plating Apparatus for Electrodeposition of Ni-SiC Composite Coatings Using Circulating-Solution Co-Deposition Technique. *J. Alloys Compd.* **2016**, *699*, 366–377. [[CrossRef](#)]
10. Shakoor, R.A.; Kahraman, R.; Waware, U.; Wang, Y.; Gao, W. Properties of Electrodeposited Ni-B-Al₂O₃ Composite Coatings. *Mater. Des.* **2014**, *64*, 127–135. [[CrossRef](#)]
11. Akbarpour, M.R.; Gharibi Asl, F.; Rashedi, H. Anti-Corrosion and Microstructural Properties of Nanostructured Ni-Co Coating Prepared by Pulse-Reverse Electrochemical Deposition Method. *J. Mater. Eng. Perform.* **2024**, *33*, 94–101. [[CrossRef](#)]
12. Vamsi MV, N.; Wasekar, N.P.; Sundararajan, G. Influence of Heat Treatment on Microstructure and Mechanical Properties of Pulse Electrodeposited Ni-W Alloy Coatings. *Surf. Coat. Technol.* **2017**, *319*, 403–414. [[CrossRef](#)]
13. Hou, K.H.; Chen, Y.C. Preparation and Wear Resistance of Pulse Electrodeposited Ni-W/Al₂O₃ Composite Coatings. *Appl. Surf. Sci.* **2011**, *257*, 6340–6346. [[CrossRef](#)]
14. Adelkhani, H.; Arshadi, M.R. Properties of Fe-Ni-Cr Alloy Coatings by Using Direct and Pulse Current Electrodeposition. *J. Alloys Compd.* **2009**, *476*, 234–237. [[CrossRef](#)]
15. Sun, J.; Du, D.X.; Lv, H.F.; Zhou, L.; Wang, Y.G.; Qi, C.G. Microstructure and Corrosion Resistance of Pulse Electrodeposited Ni-Cr Coatings. *Surf. Eng.* **2015**, *31*, 406–411. [[CrossRef](#)]
16. Firouzi-Nerbin, H.; Nasirpouri, F.; Moslehifard, E. Pulse Electrodeposition and Corrosion Properties of Nanocrystalline Nickel-Chromium Alloy Coatings on Copper Substrate. *J. Alloys Compd.* **2020**, *822*, 153712. [[CrossRef](#)]
17. Liu, C.; Huang, X.; Xu, R.; Mai, Y.; Zhang, L.; Jie, X. Microstructure and Properties of Nanocrystalline Ni-Mo Coatings Prepared by Ultrasound-Assisted Pulse Electrodeposition. *J. Mater. Eng. Perform.* **2021**, *30*, 2514–2525. [[CrossRef](#)]
18. Xu, Y.; Gao, Y.; Fan, M.; Lu, X.; Chen, Y.; Zhao, Q. Preparation and Investigation of Pulse Co-Deposited Duplex Nanoparticles Reinforced Ni-Mo Coatings under Different Electrodeposition Parameters. *Ceram. Int.* **2022**, *48*, 29629–29640. [[CrossRef](#)]
19. Rezaeiolum, A.; Aliofkhazraei, M.; Karimzadeh, A.; Rouhaghdam, A.S.; Miresmaeili, R. Electrodeposition of Ni-Mo and Ni-Mo-(Nano Al₂O₃) Multilayer Coatings. *Surf. Eng.* **2018**, *34*, 423–432. [[CrossRef](#)]
20. Zhou, X.W.; Shen, Y.F.; Jin, H.M.; Zheng, Y.Y. Microstructure and Depositional Mechanism of Ni-P Coatings with Nano-Ceria Particles by Pulse Electrodeposition. *Trans. Nonferrous Met. Soc. China* **2012**, *22*, 1981–1988. [[CrossRef](#)]
21. Zoikis-Karathanasis, A.; Pavlatou, E.A.; Spyrellis, N. Pulse Electrodeposition of Ni-P Matrix Composite Coatings Reinforced by SiC Particles. *J. Alloys Compd.* **2010**, *494*, 396–403. [[CrossRef](#)]
22. Torabinejad, V.; Aliofkhazraei, M.; Rouhaghdam, A.S.; Allahyazadeh, M.H. Electrodeposition of Ni-Fe-Mn/Al₂O₃ Functionally Graded Nanocomposite Coatings. *Surf. Eng.* **2017**, *33*, 122–130. [[CrossRef](#)]
23. Zhu, Z.; Li, X.; Zhu, D. Mechanical Electrodeposition of Ni-Mn Alloy. *Mater. Manuf. Process.* **2013**, *28*, 1301–1304. [[CrossRef](#)]
24. Ma, C.; He, H.; Xia, F.; Xiao, Z.; Liu, Y. Performance of Ni-SiC Composites Deposited Using Magnetic-Field-Assisted Electrodeposition under Different Magnetic-Field Directions. *Ceram. Int.* **2023**, *49*, 35907–35916. [[CrossRef](#)]
25. Georgescu, V.; Daub, M. Magnetic Field Effects on Surface Morphology and Magnetic Properties of Co-Ni-P Films Prepared by Electrodeposition. *Surf. Sci.* **2006**, *600*, 4195–4199. [[CrossRef](#)]
26. Afroukhteh, S.; Dehghanian, C.; Emamy, M. Preparation of the Ni-P Composite Coating Co-Deposited by Nano TiC Particles and Evaluation of It's Corrosion Property. *Appl. Surf. Sci.* **2012**, *258*, 2597–2601. [[CrossRef](#)]
27. Guo, Y.; Feng, Q.; Ma, J. The Hydrogen Generation from Alkaline NaBH₄ Solution by Using Electroplated Amorphous Co-Ni-P Film Catalysts. *Appl. Surf. Sci.* **2013**, *273*, 253–256. [[CrossRef](#)]
28. Tian, L.; Xu, J.; Qiang, C. The Electrodeposition Behaviors and Magnetic Properties of Ni-Co Films. *Appl. Surf. Sci.* **2011**, *257*, 4689–4694. [[CrossRef](#)]
29. Xia, F.; Yan, P.; Ma, C.; Zhang, Y.; Li, H. Pulse-Electrodeposited Ni/W-Al₂O₃ Nanocomposites at Different Current Densities. *J. Nanopart. Res.* **2023**, *25*, 208. [[CrossRef](#)]
30. Chen, L.; Wang, L.; Zeng, Z.; Xu, T. Influence of Pulse Frequency on the Microstructure and Wear Resistance of Electrodeposited Ni-Al₂O₃ Composite Coatings. *Surf. Coat. Technol.* **2006**, *201*, 599–605. [[CrossRef](#)]
31. Gül, H.; Uysal, M.; Akbulut, H.; Alp, A. Effect of PC Electrodeposition on the Structure and Tribological Behavior of Ni-Al₂O₃ Nanocomposite Coatings. *Surf. Coat. Technol.* **2014**, *258*, 1202–1211. [[CrossRef](#)]
32. Ghaziof, S.; Gao, W. The Effect of Pulse Electroplating on Zn-Ni Alloy and Zn-Ni-Al₂O₃ Composite Coatings. *J. Alloys Compd.* **2014**, *622*, 918–924. [[CrossRef](#)]

33. Chang, L.M.; An, M.Z.; Shi, S.Y. Microstructure and Characterization of Ni-Co/Al₂O₃ Composite Coatings by Pulse Reversal Electrodeposit. *Mater. Chem. Phys.* **2006**, *100*, 395–399. [[CrossRef](#)]
34. Fini, M.H.; Amadeh, A. Improvement of Wear and Corrosion Resistance of AZ91 Magnesium Alloy by Applying Ni–SiC Nanocomposite Coating via Pulse Electrodeposition. *Trans. Nonferr. Met. Soc. China* **2013**, *23*, 2914–2922. [[CrossRef](#)]
35. Gyftou, P.; Pavlatou, E.A.; Spyrellis, N. Effect of Pulse Electrodeposition Parameters on the Properties of Ni/Nano-SiC Composites. *Appl. Surf. Sci.* **2008**, *254*, 5910–5916. [[CrossRef](#)]
36. Sliem, M.H.; Shahzad, K.; Sivaprasad, V.N.; Shakoob, R.A.; Abdullah, A.M.; Fayyaz, O.; Kahraman, R.; Umer, M.A. Enhanced Mechanical and Corrosion Protection Properties of Pulse Electrodeposited NiP-ZrO₂ Nanocomposite Coatings. *Surf. Coat. Technol.* **2020**, *403*, 126340. [[CrossRef](#)]
37. Zhang, W.; Ji, C.; Li, B. Synthesis and Properties of Ni-W/ZrO₂ Nanocomposite Coating Fabricated by Pulse Electrodeposition. *Results Phys.* **2019**, *13*, 10224. [[CrossRef](#)]
38. Bhutta, M.U.; Khan, Z.A.; Garland, N. Wear Performance Analysis of Ni–Al₂O₃ Nanocomposite Coatings under Nonconventional Lubrication. *Materials* **2019**, *12*, 36. [[CrossRef](#)]
39. Bhutta, M.U.; Khan, Z.A. Wear and Friction Performance Evaluation of Nickel Based Nanocomposite Coatings under Refrigerant Lubrication. *Tribol. Int.* **2020**, *148*, 106312. [[CrossRef](#)]
40. John, A.; Saeed, A.; Khan, Z.A. Influence of the Duty Cycle of Pulse Electrodeposition-Coated Ni-Al₂O₃ Nanocomposites on Surface Roughness Properties. *Materials* **2023**, *16*, 2192. [[CrossRef](#)]
41. Pawlus, P.; Reizer, R.; Zelasko, W. Prediction of Parameters of Equivalent Sum Rough Surfaces. *Materials* **2020**, *13*, 4898. [[CrossRef](#)] [[PubMed](#)]
42. Bhushan, B. Surface Roughness Analysis and Measurement Techniques. In *Modern Tribology Handbook: Volume One: Principles of Tribology*; CRC Press: Boca Raton, FL, USA, 2000; pp. 49–119. [[CrossRef](#)]
43. Profile Parameters from ISO 4287—Surface Metrology Guide—Digital Surf. Available online: <https://guide.digitalsurf.com/en/guide-iso-4287-parameters.html> (accessed on 13 January 2025).
44. Dai, P.Q.; Zhong, Y.H.; Zhou, X. Corrosion Characteristic of Pulsed Electrodeposition Ni-Co/SiC Nanocomposite Coating. *Surf. Eng.* **2011**, *27*, 71–76. [[CrossRef](#)]
45. Qiao, G.; Wang, S.; Wang, X.; Chen, X.; Wang, X.; Cui, H. Preparation and Corrosion Protection Performance of a Pulse Co-Deposited Ni/Co/SiO₂ Hydrophobic Composite Coating. *ChemPhysMater* **2022**, *1*, 119–125. [[CrossRef](#)]
46. Yu, X.; Ma, Z.; Li, J.; Ma, C. Study of the Novel Ni/Co–SiC Coatings Deposited by Pulse Current Electrodeposition. Influence of the Pulse Frequency and the Duty Cycle. *Int. J. Electrochem. Sci.* **2021**, *16*, 21036. [[CrossRef](#)]
47. Yang, Y.; Cheng, Y.F. Fabrication of Ni-Co-SiC Composite Coatings by Pulse Electrodeposition—Effects of Duty Cycle and Pulse Frequency. *Surf. Coat. Technol.* **2013**, *216*, 282–288. [[CrossRef](#)]
48. Ma, C.; Zhao, D.; Ma, Z. Effects of Duty Cycle and Pulse Frequency on Microstructures and Properties of Electrodeposited Ni–Co–SiC Nanocoatings. *Ceram. Int.* **2020**, *46*, 12128–12137. [[CrossRef](#)]
49. Guglielmi, N. Kinetics of the Deposition of Inert Particles from Electrolytic Baths. *J. Electrochem. Soc.* **1972**, *119*, 1009. [[CrossRef](#)]
50. Storonkin, A.V.; Lagunov, M.D.; Beloko-skov, V.I.; Guglielmi, N. *Modern Aspects of Electrochemistry*; Plenum Press: New York, NY, USA, 1966.

Disclaimer/Publisher’s Note: The statements, opinions and data contained in all publications are solely those of the individual author(s) and contributor(s) and not of MDPI and/or the editor(s). MDPI and/or the editor(s) disclaim responsibility for any injury to people or property resulting from any ideas, methods, instructions or products referred to in the content.